

Simulation of terrestrial laser scanning errors occurring during deformation monitoring

T. Mill

Faculty of Civil Engineering, Chair of Geodesy,

Tallinn University of Technology, Ehitajate tee 5, 19086 Tallinn, Estonia, Ph. +372 620 2002

Abstract. This study estimates range and spatial distribution of terrestrial laser scanning (TLS) errors occurring at deformation monitoring. Simulations of various deformation monitoring scenarios were developed and conducted. To model realistic monitoring conditions, the simulated spatial data are distorted by introduced noise. Also factors influencing TLS results such as environment, surface properties etc. affecting the accuracy of terrestrial laser scanning are also accounted for. The simulation results are approbated with a practical case study, where vertical deformations at a static bridge load tests were determined by actual TLS survey, verified also with precise conventional point-wise surveying techniques. The modelled accuracy was estimated to be ± 3.82 mm and ± 2.99 mm at two simulated scanning locations, which are slightly larger than that achieved from the actual deformation monitoring results.

Keywords. Terrestrial laser scanning, deformation monitoring, simulation, engineering structures

1 Introduction

Terrestrial laser scanning (TLS) technology has various applications due to its capability of acquiring detailed 3D information about objects within a short time-period. TLS data enable providing a complete spatial overview of the 3D deformations of engineering structures. This may be far more significant than achieving the maximum accuracy for a small amount of pre-selected point-wise locations. Yet TLS technology is not widely used in deformation monitoring of engineering structures. The main limitations have been insufficient knowledge of the accuracy of TLS data, complexity of TLS data processing, high cost of TLS equipment and data processing software.

TLS data have been used for various engineering applications, such as for Building Information Modeling (BIM) purposes (Larsen et al. 2011, Mill et al. 2013, Bosché and Guenet 2014), surveying and monitoring of technical infrastructures (Riveiro et al. 2011, Pejić 2013, Mill et al. 2014, Nuttens et al. 2014) and in monitoring of structural deformations (González-Aguilera et al. 2008, Pesci et al. 2013, Mill et al. 2015).

Although TLS would be an appealing tool for detecting ranges and spatial distribution of deformations (due to the high resolution 3D data) of the whole surface of interest, two very challenging problems remain: (i) selecting correct and appropriate method(s) for data processing and deformation assessment; (ii) the need for alternative geodetic technology to verify the achieved results. Considering the nature of the measurement, the selection of appropriate data processing method is crucial since many data processing methods exist which all have their own distinct features affecting the final result. Although TLS have been used in various projects requiring high accuracy, it is difficult to assess the accuracy of achieved results relying solely on TLS data, still there is a need for more rigorous geodetic technology for reference (e.g. precise levelling or tacheometry).

As with traditional geodetic surveying technologies, the general problem that could set the TLS deformation monitoring at the risk of failure is unstable reference points - either natural or artificial targets (distinctive object features, retro-reflective targets, spherical targets etc.). Unstable targets affect the deformation results especially at two or multi epoch monitoring cases, especially when the time lag between epochs is long (e.g. once a year).

TLS data usage for detecting deformations often require manipulations with several different computational stages (importing from TLS, removing noise, modelling, analyzing etc.), thus making the entire workflow relatively complex and time consuming.

The aim of this study is to investigate the range and spatial distribution of terrestrial laser scanning errors occurring at a simulated deformation monitoring of an engineering structure of a bridge deck. The structure of a bridge deck was chosen to compare simulated results with a practical deformation study by Mill et al. (2015). For this purpose a direct comparison of point clouds proposed by Lague et al. (2013) is used. The method is used since it does not use data interpolation nor does it create surfaces (e.g. TIN, DEM). The method also determines orthogonal distances between two point clouds, allowing thus identify outliers.

As TLS is being often used in deformation monitoring works, this study can serve as a useful refer-

ence to help designing monitoring works and to help mitigate the effects of instrumental errors. It also explains an example of assessment of errors occurring at monitoring of an object at distinct scanning locations.

Outline of the paper is as follows. The introduction is followed by overview of TLS error sources. The methods of detecting deformations using TLS data are reviewed in third section. The fourth section describes the simulation of point cloud data and noise assigning principles. The modelling results are described in the fifth section. The sixth section provides a verification with a practical case study. A brief summary concludes the paper.

2 Terrestrial laser scanning uncertainties

Since this study investigates errors occurring at deformation monitoring of engineering structures it is vital to review all possible error sources. As any other surveying technology the TLS is also affected by different sources of errors – related to object properties, operator, equipment, surveying methods and the surveying environment.

Object related errors can be associated with the object's physical properties such as color, reflectivity, roughness, temperature, moisture level, etc. (Kersten et al. 2005, Pesci and Teza 2008, Lichti 2010, Soudarissanane et al. 2011, Roca-Pardiñas et al. 2014).

Operator related errors can be associated with the operator's theoretical and practical background on surveying. These errors also include data processing (registration of point clouds, removing of unnecessary data, modelling, etc.) (Bae et al. 2005, Pesci et al. 2011).

Ideally equipment should be differentiated by object's nature and the expected results (Schulz 2007, Reshetyuk 2010).

Surveying methods are key factors in the quality and accuracy of the surveying results. These errors are affected by e.g. the scanner's orientation methods on the field, scanning resolution (Alba and Scaioni 2007, Kang et al. 2009, Franaszek et al. 2009, Bosché 2012).

Environmental errors are mainly associated with the environmental effects (humidity, dusty environments, temperature, etc.) to the scanning device (Pfeifer et al. 2007, Borah and Voelz 2007).

Each of mentioned error factors contribute to the error budget of TLS surveys.

3 Methods for detecting deformations

Four of the most common methods for detecting deformations using TLS data are explained below.

1) Assessing deformations by comparing surfaces created using digital elevation models (DEM) or triangulated irregular networks (TIN) originating from different surveying epochs (Zogg and Ingensand 2008, Riveiro et al. 2011, Mill et al. 2014, 2015). Both DEM and TIN models are sensitive to point cloud roughness, missing data (e.g. hidden parts) and outliers which are subject to surface interpolation, thus effecting the assessment of deformations.

2) Assessing deformations by comparing simple geometrical shapes like planes, cylinders or spheres. The fitting of a geometrical shape into a point cloud can be processed in two ways: (i) least squares fitting (Park and Lee 2007); (ii) non-iterative fitting where the shapes are described by a few parameters (Erdélyi et al. 2014). In fitting simple geometrical shapes problems arise with choosing the correct mathematical model into which the point clouds from different sets of data are fitted into. This is due to circumstance that generally no simple and unambiguous surfaces exist which could be accurately defined.

3) Assessing deformation through least squares surface matching (Montserrat and Crosetto 2008, Opijkofer et al. 2009). The method provides 3D deformation parameters, displacement vectors and rotations, of the deformed object. Nevertheless the method is sensitive to surfaces which have partially deformed.

4) Assessing deformations directly using point clouds, also known as cloud to cloud methods: (i) using the nearest neighbours averaging technique (Abellán et al. 2009); (ii) using the minimal distance projection method (Han et al. 2013); (iii) measuring orthogonal distances between two point clouds (Lague et al. 2013). The benefit of mentioned methods is that they do not require any intermediate data processing and the methods work in 3D.

This study implements the direct comparison of point clouds proposed by Lague et al. (2013). The method uses 3D surface normal estimation at a scale consistent of surface roughness and calculates dis-

tances along normal direction between comparable point clouds.

4 Simulated TLS data

Simulated TLS data has been developed for a lower side of a bridge deck. The simulated bridge deck is a simplified model without the deck camber and beams. The opening span of the simulated bridge deck is exactly 60 m and the width of the deck is exactly 10 m. The point density of 0.10 m, was chosen to simplify the computations, thus the simulated surface consists of 60 701 survey points.

The coordinates of the survey points in the laser scanner's intrinsic coordinate system $(\Delta x_i, \Delta y_i, \Delta z_i)$ were generated. The spherical coordinates of the point cloud are computed by the well-known relations in-between rectangular coordinates and spherical coordinates

$$\begin{bmatrix} \Delta x_i \\ \Delta y_i \\ \Delta z_i \end{bmatrix}_{i=1..n} = \begin{bmatrix} \rho_i \cos \theta_i \cos \varphi_i \\ \rho_i \sin \theta_i \cos \varphi_i \\ \rho_i \sin \varphi_i \end{bmatrix}, \quad (1)$$

where ρ_i is the range to the object surface from the scanner's centre, θ_i is the horizontal angle with respect to initial direction and φ_i is the vertical angle from horizon.

The simulated data consists in total of four sets (two for each epoch) of point clouds acquired from two distinct scanner locations in respect to the bridge deck. The scanning stations are located: (i) under the bridge at the centre of the bridge deck (station B1); (ii) at the side of the bridge deck at the horizontal distance of 6 m away from the deck (station B2) (Figure 1). In both cases the vertical distance from the scanner centre to the level of the bridge lower surface is 4.3 m.

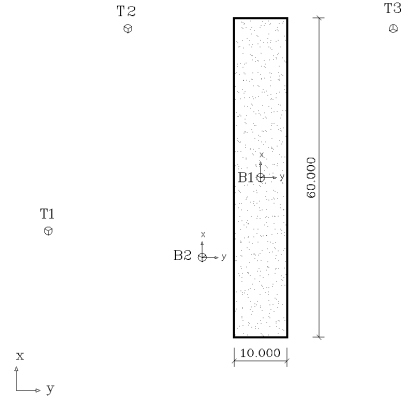


Fig. 1 Top view of the locations of the scanning stations (B1 and B2) and targets (T1, T2, T3) on the lower side of the bridge deck. The coordinate system axes are depicted at left. Units are in meters.

4.1 Simulated TLS data errors

In order to model realistic deformation monitoring conditions, the data are artificially contaminated by measurement noise:

Firstly, errors for each survey point at the level of 1σ confidence interval were calculated using the equation of the combined standard uncertainty with independent quantities:

$$\sigma^2(\hat{P}) = \sum_{i=1}^n \left(\frac{\partial f_n}{\partial w_i} \right)^2 \sigma^2(w_i), \quad (2)$$

where $\sigma^2(\hat{P})$ denotes the variance of the survey point determined by TLS. Note that \hat{P} is an estimate of the actual survey point P stemming from the TLS range and angle measurements, f_n is the function $P=f_n(w_i), i=1, \dots, n$, relating the observations $(w_i), i=1, \dots, n$. The notation \hat{P} represents a general notation for the 3D position of the point in order to distinguish it from the specific x , y and z -coordinate. $\sigma^2(w_i)$ is the standard error of an i -th observable, where (σ_{dist}) was taken 0.004 m, the horizontal angle $(\sigma_{h.angle})$ and vertical angle $(\sigma_{v.angle})$ uncertainties were taken 12'' (arc-second) (typical for many up-to-data TLS devices).

Secondly, based on the sizes of the calculated standard uncertainty values, survey errors at 3σ confidence interval were introduced under the condition of normal distribution ($\varepsilon \sim N(0,1)$).

As in actual deformation monitoring situation, the scanner's intrinsic coordinate system is oriented before the second monitoring session (II scanning

epoch) to acquire data in the same coordinate system as in the first epoch. For orientation, only stable targets should be used. The latter is vital to mitigate additional errors due to scanner orientation. Since target acquisition errors are generally smaller than of the single point errors, than the introduced target measuring errors are considered three times smaller than that of the common survey points.

For the size of the simulated deformation, the bridge deck surface was deflected at the centre part for -0.0150 m (Figure 2). Even though several international standards related to construction deformations are available (e.g. ISO 2394 design and assessment of structures, ISO 13822 assessment of existing structures, ISO 14963 guidelines for dynamic tests on bridges and viaducts, ISO 18649 evaluation of results from dynamic tests and investigations on bridges and viaducts etc.), generally no fixed deformation limits exist for static load tests. Hereby it is worth mentioning that e.g. in Mill et al. (2015) TLS yielded a maximum deflection of -3.2 cm. In the simulation case the simulated deformation is quite small which could be difficult to be detected by TLS, but is noticeable for other geodetic methods, thus it is of interest to study the achievable limits of TLS under certain theoretical conditions. The simulated deformation data was also distorted by noise as described earlier.

In terms of simplification, noise were introduced only for the (along plumb-line) z-coordinate component and for the (along-bridge) x coordinate component. The y-component is irrelevant, since during the deformations no across-bridge deflections are expected. Recall, that as the surface is deflected in the second epoch, both x and z-components are affected in sense of surface normal direction, the deck is deflected along the longitudinal direction which coincides with x-axis direction. The distributions of the combined standard uncertainties of the relevant z-component are depicted in Figure 3.

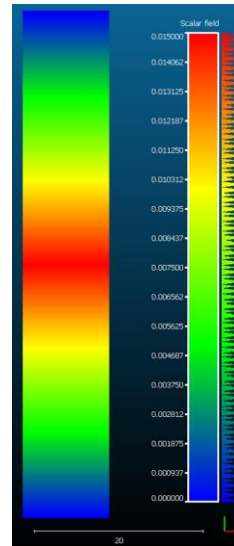


Fig. 2 Bridge deck with deflection at the center part for -0.0150 m. Note the scale and the deflection distribution histogram at the right. Coordinate axes is depicted in the bottom right corner, where green indicating x-axis, red indicating y-axis.

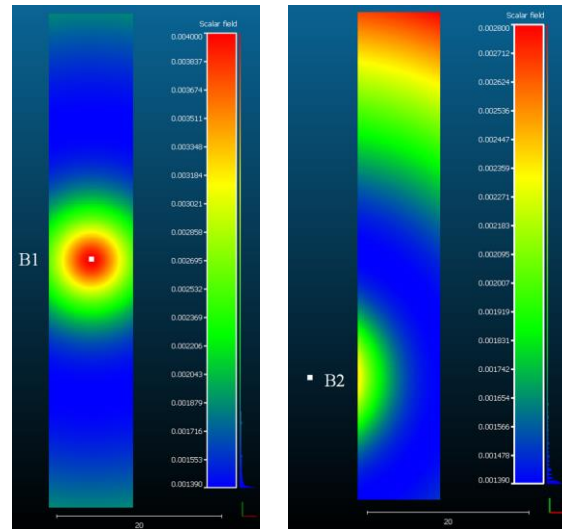


Fig. 3 Distribution of calculated combined standard uncertainty values for z coordinate component for two scanning locations B1 and B2 (denoted by white dots on the left-hand and right-hand figures, respectively).

As can be seen from Figure 3, the highest standard uncertainty values in z-component (0.00400 m) are when the scanner is directly under the bridge deck at station B1 (Figure 3 left). The main cause for this is that from that location the accuracy of the survey point is affected only by the distance measur-

ing accuracy (recall $\sigma_{\text{dist}} = 0.004$ m). At station B1 the angle of incidence value of the laser beam is zero directly above the scanner. The angle of incidence values vary from 0° to approximately 80° (arc-degrees) across the surface (cf. section 3).

At the scanning station B2 (Figure 3 right), the standard uncertainty values do not exceed 0.00280 m, which is due the fact that the survey point error is affected at lesser extent by both the distance measuring accuracy and angular accuracy. In this case the angle of incidence of the laser beam is between approximately 55° to 85° across the surface.

Based on the calculated combined standard uncertainty values it is expected that detecting deformations from scanner station B1 is more affected by surveying errors than in station B2.

5 Results

5.1 Transformation of the bridge deck data

The calculated RMS (equation 3) values of the transformed target coordinates of the simulated monitoring data from the second epoch into the first epoch are presented in Table 1. The RMS values of the z-component are under one millimetre level in both cases at scanning stations B1 and B2.

$$RMS = \pm \sqrt{\frac{\sum_{i=1}^n \varepsilon_i^2}{n}}, \quad (3)$$

where ε_i is error, n is the number of points.

Table 1. Calculated RMS values of the transformed target coordinates from the second epoch into the first

	RMS _x	RMS _z
B1 II epoch into I	0.00295	0.00003
B2 II epoch into I	0.00175	0.00001

The transformation i.e. registration of point clouds from the second epoch into the first is carried out using the transformation parameters (rotations \mathbf{R} and translations \mathbf{T}) calculated in transformation of target coordinates.

The coordinate transformation was proceeded by 3D rigid body transformation:

$$\mathbf{g}_i = \mathbf{R}\mathbf{m}_i + \mathbf{T}, \quad (4)$$

where $\{\mathbf{m}_i\}$ and $\{\mathbf{g}_i\}$, $i=1, \dots, n$ are two sets of common points e.g. lasers canning targets, \mathbf{R} is rotation matrix, \mathbf{T} is a translation vector.

For estimating the optimal transformation parameters, rotation (\mathbf{R}) and translation (\mathbf{T}), the closed-form solution, introduced by Horn (1987), was used. The method uses the unit quaternions instead of orthonormal matrix to represent rotation. The optimal transformation parameters are found by the least squares criterion:

$$\varepsilon_{\text{min}}^2 = \sum_{i=1}^n \|\mathbf{g}_i - \hat{\mathbf{R}}\mathbf{m}_i - \hat{\mathbf{T}}\|^2 \quad (5)$$

To assess the effects of transformation to the relevant coordinate components (x, and z) separately, data transformation was proceeded with transformation parameters without introduced noise. RMS values were calculated using the differences of each coordinate component, transformed with erroneous parameters and with error free parameters. The resulted RMS values are depicted in Figure 4. The overall RMS_{x,z} of the relevant coordinate components together is found by:

$$RMS_{x,z} = \sqrt{RMS_x^2 + RMS_z^2} \quad (6)$$

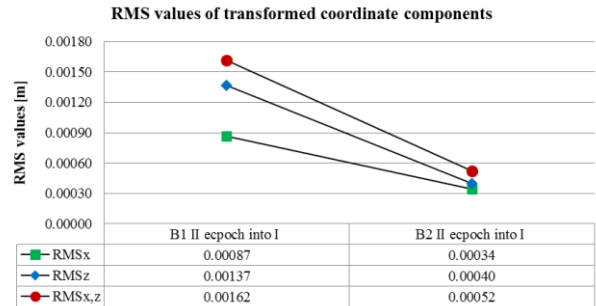


Fig. 4 RMS values of differences of transformed data with erroneous transformation parameters and error free transformation parameters.

As shown in Figure 4, RMS values are generally somewhat higher in scanning station B1. The RMS value in z-component at station B1 (± 0.00137 m) is considerably higher than in station B2 (± 0.00040 m), the latter has relevant influence in the assessment of deformations. The higher RMS values in z-component are probably due to the scanner location in respect to the object where the point cloud is more distorted by distance measuring errors ($\sigma_{\text{dist}} = 0.004$ m, cf. Figure 3). The RMS values in x-

component in station B1 are at sub millimetre level thus having marginal or no influence in the assessment of deformations.

The results of transformation of the second data from station B2 show only sub millimetre RMS values at x and z-component.

The assessment of the effects of transformation to each coordinate component also indicated that deformation monitoring result should be more accurate from station B2 that is located at the side of the bridge deck.

5.2 Noise level

The simulated data in the first scanning epochs, when the surface was not deformed, errors were introduced only for the crucial z-coordinate component. The RMS values of the noise level in z-components were ± 0.00252 m and ± 0.00209 m for stations B1 and B2, respectively.

To assess the overall magnitudes of the measuring noise level of the simulated data of the second epochs, RMS values were calculated based on the point clouds free of all errors and point clouds with errors. In addition, these clouds were also affected by transformation (Figure 5).

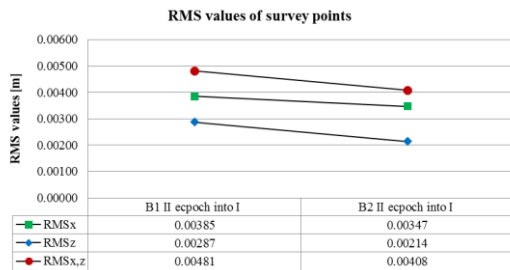


Fig. 5 RMS values of differences of error free data and erroneous data.

The RMS values in Figure 5 show that both data sets suffer from somewhat identical noise magnitudes. As the nature of the deformation in the simulated bridge deck is in the direction of z-axis, the noise level in z-component is most crucial.

The overall noise level of the I and II epochs is calculated by equation (6) using the z-component RMS values of each epoch. The results appeared to be ± 0.00382 and ± 0.00299 m for scanning station B1 and B2, respectively.

5.3 Assessment of deformations of the bridge deck

For deformation assessment point clouds from two simulated scanning epochs were compared using the method proposed by Lague et al. (2013). The results of the comparisons of the two scanning epochs from separate scanning locations (B1 and B2) are depicted in Figure 5.

Although clearly the spatial distribution of the comparisons are well noticeable between the two scanning locations (B1 and B2), the magnitudes of the deflections are both within reasonable sizes (see Table 2). Nevertheless, since the actual size and the distribution of the deformation is known, the distribution and the nature of the detected deformation from station B2 is more equivalent to the true deformation (-0.0150 m cf. Figure 2). The latter can be associated with larger angle of incidence values where the instrument's distance measuring accuracy has less effects in the accuracy of the survey point as in the case of surveying in the perpendicular direction.

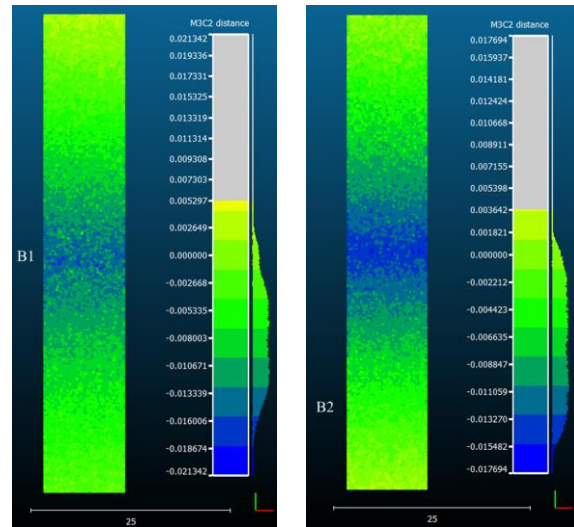


Fig. 6 Comparison of the simulated bridge deck surface. Figure A illustrates the comparison of the I and the II epoch data in the case where the scanner (B1) is located directly under the bridge deck. Figure B illustrates the comparison of the I and the II epoch data in the case where the scanner (B2) is located at the side of the bridge deck. Note the grey areas on the scale bars which indicates no values.

In Table 2, the achieved minimum and maximum results confirm with previous assessments, that from

location B1 the data comparison displays more noise than from location B2. Thereby other statistics are also slightly higher, which also confirms the existence of higher noise level.

Table 2. Statistics of the comparison (Figure 6) of deflected and without deflection bridge deck data

Station	Min [m]	Max [m]	μ [m]	RMS [m]
B1	-0.02134	0.00530	-0.00795	0.00470
B2	-0.01769	0.00364	-0.00729	0.00444

6 Practical case

A practical study of monitoring of deformations with a TLS of a reinforced concrete cantilever bridge was carried out in 2013 (Mill et al. 2015).

The monitoring process with a TLS was carried out at the side location of the bridge at a safety distance due the risk of collapse of the structure. Similarly to the simulated deformation monitoring case the scanner was reoriented before each TLS session to ensure the stability of the scanner.

Results from Mill et al. (2015) indicated that the achieved accuracy of TLS deformation monitoring was ± 2.8 mm. In this case the angle of incidence values were assessed to be 80-87°. The achieved TLS results were verified by high-precision leveling.

The results in Mill et al. (2015) indicated that the deformations of the beams of the bridge were homogeneous by nature in both longitudinal directions when moving away from the loading point. The beams deformed into an arch shape structures, similar deformation characteristics were detected in the simulation (Figure 5) at scanner station B2. The distribution of the deformation over the concerned area is uniform in both longitudinal direction and is easily to recognize

7 Conclusions

This paper focused on a theoretical study of the accuracy of monitoring deformations with a terrestrial laser scanner with modelled accuracy parameters.

The simulation results showed that smaller surveying errors are achieved when deformation monitoring is carried out from locations where the angle of incidence of the laser beam is greater than 50° (arc-degrees), thus the instrument's angular and

distance measuring accuracies affect the accuracy of the survey point at lesser extent. The latter is well described by the maximum values of the calculated combined standard uncertainty values in z-component 0.00400 m and 0.00280 m for stations B1 m and B2, respectively.

The introduced noise level at 3σ confidence interval level of stations B1 m and B2 at the first epoch were ± 0.00252 m and ± 0.00209 m, respectively. At the second epoch, the noise levels were calculated to be ± 0.00287 m and ± 0.00214 m for stations B1 and B2, respectively. The overall magnitude of noise level of the I and II epochs after transformation is ± 0.00382 and ± 0.00299 m, respectively.

The assessed noise level in z-component of the simulated deformation monitoring showed slightly lower accuracy (± 0.00299 m) than in the practical case in Mill et al. (2015), where the verified accuracy was ± 2.8 mm. Both results were achieved at the side location of the objects. The assessed noise level at simulated station B1 located under the bridge was ± 0.00382 m.

The study also revealed that the nature of the deformation from location B2 is similar to the nature of the deformation found in Mill et al. (2015).

In future monitoring projects it is advisable to choose the laser scanner location based on the expected angle of incidence values and to avoid surveying perpendicular to the object. The study showed that using a laser scanner with given accuracy specifications ($\sigma_{dist} = 0.004$ m, $\sigma_{h,angle}$ and $\sigma_{v,angle} = 12''$) for monitoring purposes the achievable accuracies are above two millimetre level.

References

- Abellán, A., Jaboyedoff, M., Oppikofer, T., Vilaplana, J. M. (2009). Detection of millimetric deformation using a terrestrial laser scanner: experiment and application to a rockfall event. *Natural Hazards and Earth System Sciences*, 9, pp. 365 - 372.
- Alba, M., Scaioni, M. (2007). Comparison of techniques for terrestrial laser scanner data georeferencing applied to 3-D modeling of cultural heritage. In: *Proc. 3D-ARCH 2007: "Virtual Reconstruction and Visualization of Complex Architectures"*, Zurich, Switzerland, ISPRS, pp. 1 - 8.
- Bae, K.-H., Belton, B., Lichti, D. D. (2005). A framework for position uncertainty of unorganised three-dimensional point clouds from near-monostatic laser scanners using covariance analysis. *ISPRS Workshop "Laser scanning 2005"*, Enschede, Netherlands, ISPRS, pp. 7 - 12.

- Borah, D. K., Voelz, D. G. (2007). Estimation of laser beam pointing parameters in the presence of atmospheric turbulence. *Applied Optics*, 46(23), pp. 6010 - 6018.
- Bosché, F. (2012). Plane-based registration of construction laser scans with 3D/4D building models. *Advanced Engineering Informatics*, 26(1), pp. 90 - 102.
- Bosché, F., Guenet, E. (2014). Automating surface flatness control using terrestrial laser scanning and building information models. *Automation in Construction*, 44, pp. 212 - 226.
- Erdélyi, J., Kopáčík, A., Ilkovičová, E., Lipták, I., Kajánek, P. (2014). Deformation Monitoring of a Parabolic Roof Structure using TLS. In: *Proc. "INGEO 2014"*, Prague, Czech republic, pp. 75 - 80.
- Franaszek, M., Cheok, G. S., Witzgall, C. (2009). Fast automatic registration of range images from 3D imaging systems using sphere targets. *Automation in Construction*, 18(3), pp. 265 - 274.
- González-Aguilera, D., Gómez-Lahoz, J., Sánchez, J. (2008). A New Approach for Structural Monitoring of Large Dams with a Three-Dimensional Laser Scanner. *Sensors*, 8(9), pp. 5866 - 5883.
- Han, J.-Y., Guo, J., Jiang, Y.-S. (2013). Monitoring tunnel deformations by means of multi-epoch dispersed 3D LiDAR point clouds: An improved approach. *Tunnelling and Underground Space Technology*, 38, pp. 385-389.
- Horn, B. K. (1987). Closed-form solution of absolute orientation using unit quaternions. *Journal of the Optical Society of America*, 4(4), pp. 629 - 642.
- Kang, Z., Li, J., Zhang, L., Zhao, Q., Zlatanova, S. (2009). Automatic registration of terrestrial laser scanning point clouds using panoramic reflectance images. *Sensors*, 9(4), pp. 2621 - 2646.
- Kersten, T. P., Sternberg, H., Mechelke, K. (2005). Investigations into the accuracy behaviour of the terrestrial laser scanning system Mensi GS100. In: *Proc. "Optical 3-D Measurement Techniques VII"*, Vienna, Austria, pp. 122 - 131.
- Lague, D., Brodu, N., Leroux, L. (2013). Accurate 3D comparison of complex topography with terrestrial laser scanner : application to the Rangitikei canyon (N-Z). *ISPRS Journal of Photogrammetry and Remote Sensing*, 82, pp. 10 - 26.
- Larsen, K. E., Lattke, F., Ott, S., Winter, S. (2011). Surveying and digital workflow in energy performance retrofit projects using prefabricated elements. *Automation in Construction*, 20(8), pp. 999 - 1011.
- Lichti, D. D. (2010). Terrestrial laser scanner self-calibration: Correlation sources and their mitigation. *ISPRS Journal of Photogrammetry and Remote Sensing*, 65(1), pp. 93 - 102.
- Mill, T., Alt, A., Liias, R. (2013). Combined 3D building surveying techniques – terrestrial laser scanning (TLS) and total station surveying for BIM data management purposes. *Journal of Civil Engineering and Management*, 19(1), pp. 1 - 10.
- Mill, T., Ellmann, A., Aavik, A., Horemuz, M., Sillamäe, S. (2014). Determining ranges and spatial distribution of road frost heave by terrestrial laser scanning. *The Baltic Journal of Road and Bridge Engineering*, 9(3), pp. 227 - 236.
- Mill, T., Ellmann, A., Kiisa, M., Idnurm, J., Idnurm, S., Horemuz, M., Aavik, A. (2015). Geodetic Monitoring of Bridge Deformations Occurring during Static Load Testing. *The Baltic Journal of Road and Bridge Engineering*, 10(1), pp. 17 - 27.
- Monserrat, O., Crosetto, M. (2008). Deformation measurement using terrestrial laser scanning data and least squares 3D surface matching. *ISPRS Journal of Photogrammetry and Remote Sensing*, 63(1), pp. 142 - 154.
- Nuttens, T., Stal, C., De Backer, H., Schotte, K., Van Bogaert, P., De Wulf, A. (2014). Methodology for the ovalization monitoring of newly built circular train tunnels based on laser scanning: Liefkenshoek Rail Link (Belgium). *Automation in Construction*, pp. 43, 1 - 9.
- Oppikofer, T., Jaboyedoff, M., Blikra, L., Derron, M.-H., Metzger, R. (2009). Characterization and monitoring of the Åknes rockslide using terrestrial laser scanning. *Natural Hazards and Earth System Sciences*, 9, pp. 1003 -1019.
- Park, H. S., Lee, H. M., Adeli, H., Lee, I. (2007). A New Approach for Health Monitoring of Structures: Terrestrial Laser Scanning. *Computer-Aided Civil and Infrastructure Engineering*, 22(1), pp. 19 - 30.
- Pejić, M. (2013). Design and optimisation of laser scanning for tunnels geometry inspection. *Tunnelling and Underground Space Technology*, 37, pp. 199 - 206.
- Pesci, A., Teza, G. (2008). Terrestrial laser scanner and retro-reflective targets: an experiment for anomalous effects investigation. *International Journal of Remote Sensing*, 29(19), pp. 5749 - 5765.
- Pesci, A., Casula, G., Boschi, E. (2011). Laser scanning the Garisenda and Asinelli towers in Bologna (Italy): Detailed deformation patterns of two ancient leaning buildings. *Journal of Cultural Heritage*, 12(2), pp. 117 - 127.
- Pesci, A., Teza, G., Bonali, E. (2011). Terrestrial Laser Scanner Resolution: Numerical Simulations and Experiments on Spatial Sampling Optimization. *Remote Sensing*, 3(1), pp. 167 - 184.
- Pesci, A., Teza, G., Bonali, E., Casula, G., Boschi, E. (2013). A laser scanning-based method for fast estimation of seismic-induced building deformations. *ISPRS Journal of Photogrammetry and Remote Sensing*, 79, pp. 185 - 198.
- Pfeifer, N., Dorninger, P., Haring, A., Fan, H. (2007). Investigating terrestrial laser scanning intensity data quality and functional relations. In: *Proc. "International Conference on Optical 3-D Measurement Techniques VIII"*, Zurich, Switzerland, pp. 328 - 337
- Reshetyuk, Y. (2010). A unified approach to self-calibration of terrestrial laser scanners. *ISPRS Journal of Photogrammetry and Remote Sensing*, 65(5), pp. 445-456.
- Riveiro, B., Morer, P., P., A., I. de Arteaga, I. D. (2011). Terrestrial laser scanning and limit analysis of masonry arch bridges. *Construction and Building Materials*, 25(4), pp. 1726 - 1735.
- Roca-Pardiñas, J., Argüelles-Fraga, R., López, F. d., Ordóñez, C. (2014). Analysis of the influence of range and angle of incidence of terrestrial laser scanning measurements on tunnel inspection. *Tunnelling and Underground Space Technology*, 43, pp. 133 - 139.
- Soudarissanane, S., Lindenbergh, R., Menenti, M., Teunissen, P. (2011). Scanning geometry: Influencing factor on the quality of terrestrial laser scanning points. *ISPRS Journal of Photogrammetry and Remote Sensing*, 66(4), pp. 389 - 399.

Zogg, H.-M., Ingensand, H. (2008). Terrestrial laser scanning for deformation monitoring - load tests on the felsenau viaduct (CH). In: *Proc. ISPRS Congress "Silk Road for Information from Imagery"*, Beijing, China pp. 555 - 562.